

Research Article

Modulating the Shape and Size of Backprojection Surfaces to Improve Accuracy in Volumetric Stereo

X. Zabulis and G. D. Floros

Institute of Computer Science, Foundation for Research and Technology-Hellas, N. Plastira 100, Vassilika Vouton, 700 13 Heraklion, Crete, Greece

Correspondence should be addressed to X. Zabulis, zabulis@ics.forth.gr

Received 14 October 2007; Accepted 7 April 2008

Recommended by John Watson

In 3D TV applications, the extraction of 3D representations of dynamic scenes from images plays a central role in the preparation of the presented visual content. This paper focuses on the stereo cue to the extraction of these representations and, in particular, on the recently developed family of volumetric approaches to stereo. Two methods are proposed that improve the accuracy of volumetric stereo approaches, which compare backprojections of image regions to establish stereo correspondences. The proposed methods are based on maximizing the utilization of the available image resolution, as well as, equalizing the sampled image area across pairs of image regions that are compared.

Copyright © 2009 X. Zabulis and G. D. Floros. This is an open access article distributed under the Creative Commons Attribution License, which permits unrestricted use, distribution, and reproduction in any medium, provided the original work is properly cited.

1. Introduction

The goal of 3D television demands for high-quality and free-viewpoint visualization of a dynamic scene. Besides advances in transmission, visualization, and displays, a critical aspect of this technology is the automatic preparation of the 3D content to be shown. In this paper, efforts towards the more accurate reconstruction of scenes are presented.

The requirement of realistic free-viewpoint visualization of 3D content demands knowledge of scene geometry, in order to cope with occlusions and motion parallax. This knowledge refers to estimating at least the locations at the surfaces of the imaged scene (if not the corresponding surface normals too) and is called the *reconstruction* of the scene. Therefore, the demand for high-quality visual content underscores the need for accurate extraction of such scene reconstructions. Approaches that synthesize views (e.g., [1]) instead of reconstructing the imaged structure are not considered in the context of this work, as they exhibit limited treatment of occlusions.

This paper focuses on the 3D reconstruction of imaged scenes and, in particular, in the cue to scene geometry due to the assumption of texture uniqueness. The initial formulation of this cue stated that a given pixel from one image can match to no more than one pixel from the other

image [2, 3], however, it has been recently updated [4] to apply for more general configurations of the imaged surfaces as well as their apparent shape. Despite the growth of methods that utilize spectral information (color) or silhouettes to reconstruct scenes, the depth cue due to the texture uniqueness constraint remains central in several modern stereo algorithms (see for a review [5]). This is due to a number of reasons including its independence on assumptions in camera position and image segmentation (see Section 2). Certainly, combination with other cues is necessary for maximizing the quality of the reconstruction, since they provide additional information and since the texture-uniqueness cue exhibits well-known weaknesses, on top of being nonoperational at textureless areas. The goal of this work is to provide of a prolific, in terms of accuracy, precision and efficiency, approach to the utilization of the texture uniqueness constraint which can be, thereafter, combined with other cues to scenes geometry.

The formulation of the texture uniqueness cue in world, rather than image, coordinates gave rise to volumetric stereo approaches, which are overviewed in Section 2. In such approaches, the acquired images are backprojected on a hypothetical backprojection surface prior to the establishment of stereo correspondences, in order to enhance the robustness of the process. In this context, it is proposed

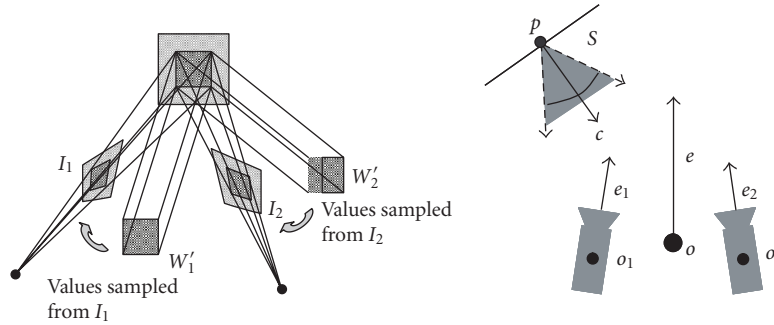


FIGURE 1: Left: A surface is projectively distorted in images $I_{1,2}$, but the collineations $w'_{1,2}$ from a planar patch tangent to this surface are not. Right: Illustration of the discussed binocular camera system geometry.

that

- (1) maximizing the image area that a unit of backprojection surface area corresponds to, and
- (2) utilizing the same amount of image area across pairs of image regions that are compared to

increases the accuracy of estimations of surface location and orientation, which is the essential information for the reconstruction of the imaged scene. The above proposals imply spatial normalizations in the comparison of backprojected image segments. Below, these normalizations are explained and studied in a separate section each; first by being theoretically formulated and then by being experimentally compared with conventional approaches.

The remainder of this paper is organized as follows. In Section 2, the stereo techniques that are related to the proposed methods are reviewed and the notation utilized in this paper is introduced. In Section 3, the first proposal is applied to the family of space-sweeping algorithms. In Section 4, the second proposal is applied to more generic cases of volumetric stereo, which utilize the estimation of the surface normal in the stereo reconstruction process. In Section 5, the results are discussed and the proposed methods are placed in the context of automatic reconstruction of visual scenes.

2. Related Work

The literature review of this section is focused at implementations of the texture uniqueness cue in stereo that compare image regions after their backprojection to establish correspondences, or else volumetric stereo approaches. A comprehensive review of the broad literature on stereo algorithms can be found in [5] and an evaluation of contemporary stereo systems in [6].

The reasons for the wide applicability of the texture uniqueness cue to the problem of stereo reconstruction of scenes are multiple. It is independent from silhouette-extraction which, also, requires an accurate segmentation (e.g., [7]). It is also independent of any assumption requiring that cameras occur around the scene (e.g., [8]) or on the same baseline (e.g., [9, 10]). Moreover, it does not require that cameras are spectrally calibrated, such as in voxel

carving/coloring approaches (e.g., [11–13]). In addition, the locality of the cue due to the uniqueness constraint facilitates multiview and parallel implementations, for real-time applications [14–17].

Despite its locality, the uniqueness cue has been utilized in semilocal [18] or more global formulations; for example, via energy minimization [9, 19, 20] or dynamic programming [21]. In these methods, a local similarity operator is still utilized either as an oriented backprojection surface segment (e.g., [18]) or as an image neighborhood (e.g., [9]), but interpreted differently by fusing its readings with the well-established constraints on surface continuity. Thus, regardless of how the readings of the similarity operator are utilized by the reconstruction algorithm, the proposed accuracy enhancement of the operator should only improve the accuracy of the above approaches.

Methods that backproject and, then, compare the acquired images can be classified based on if the (estimated) orientation of the imaged surface is considered in the backprojection process [18, 22–24], or not [25–30]. These two classes are often, respectively, referred to as *volumetric* and *space-sweeping* approaches. The notation and geometry of this operation are first introduced.

Let I_1 and I_2 be the images of a calibrated image pair, acquired from two cameras with centers $\vec{o}_{1,2}$ and principal axes $\vec{e}_{1,2}$; cyclopean eye is at $\vec{o} = (\vec{o}_1 + \vec{o}_2)/2$ and mean optical axis is $\vec{e} = (\vec{e}_1 + \vec{e}_2)/2$. Let also a planar and square *backprojection surface* \mathcal{S} , of size $\alpha \times \alpha$, centered at \vec{p} , with unit normal \vec{n} . Backprojecting I_i onto \mathcal{S} yields *image collineations* $w_i(\vec{p}, \vec{n})$:

$$w_i(\vec{p}, \vec{n}) = I_i(P_i \cdot (\vec{p} + R(\vec{n}) \cdot [x' \ y' \ 0]^T)), \quad (1)$$

where P_i is the projection matrix of I_i , $R(\vec{n})$ is a rotation matrix so that $R(\vec{n}) \cdot [0 \ 0 \ 1]^T = \vec{n}$ and $x', y' \in [-\alpha/2, \alpha/2]$ are local coordinates on \mathcal{S} . When \mathcal{S} is tangent at a world surface, w_i are identities of the surface pattern (see Figure 1 (left)). Thus $I_1(P_1 \vec{x}) = I_2(P_2 \vec{x})$, for all $\vec{x} \in \mathcal{S}$, and therefore their similarity is optimal. Otherwise w_i are dissimilar, because they are collineations from different surface regions. Scene reconstruction can be obtained by detecting the positions at which the above similarity is high (greater than threshold τ) and locally maximized along the direction of the surface normal [23].

This volumetric similarity function s is computed at each point in the reconstruction volume as

$$s(\vec{p}) = \max_{\vec{n}} (\text{sim}(w_1(\vec{p}, \vec{n}), w_2(\vec{p}, \vec{n}))), \quad (2)$$

$$\vec{\kappa}(\vec{p}) = \arg \max_{\vec{n}} (s(\vec{p})), \quad (3)$$

where $s(\vec{p})$ is the optimal similarity value at \vec{p} , and $\vec{\kappa}(\vec{p})$ is the optimizing orientation. To evaluate sim , an $r \times r$ lattice of points is assumed on \mathcal{S} and the similarity metric sim is usually one of the following: SAD, SSD, NCC, MNCC [31], or photoconsistency [32]. (See [33] for a comparison of the use of these metrics in stereo vision. Based on this work, the MNCC metric is selected and, henceforth, utilized in this paper.) The parameterization of \vec{n} requires two dimensions which are expressed in terms of longitude and latitude. Henceforth, a line from a camera at \vec{o} to some point \vec{p} will be referred to as a *line of sight*, from the camera to \vec{p} .

Volumetric approaches exhibit increased accuracy over conventional epipolar-based stereo approaches, because the comparison of image collineations is relieved of projective distortion, and thus corresponding counterparts can be more robustly detected in the acquired images. In multiview stereo, there is no single notion of “depth,” and thus a world-coordinate parameterized representation is required. In this respect, volumetric approaches are very well suited for the multicamera reconstruction of scenes. On the other hand, they are computationally more complex due to the optimization of orientation κ . To reduce the exhaustive search of the above search space, the computation can be progressively guided from coarse to fine scales [17], or constrained based on the assumption that surfaces are continuous [9, 18, 20]. In such approaches, α has been generally formulated as constant [18, 22–24]. In [23, 24], α is modulated for the purpose of a computational acceleration, through a hierarchical multiresolution search. However, this modulation is identical for any location and orientation of \mathcal{S} and refers to the granularity by which the reconstruction volume is sampled. In other words, the proposed size-modulation (in Section 4) is independent, and thus applicable to the above acceleration approaches as an extension.

As shown in the next section, *space* or *plane-sweeping* approaches are a special case of the above volumetric formulation, in which only one potential orientation of \vec{n} is considered. In these approaches, a planar backprojection surface is translated (swept) along depth and the acquired images are backprojected on, and then locally compared. The orientation and shape of the sweeping surface is a priori determined independently to the actual structure of the imaged scene. Typically, orientation coincides with the viewing direction, although multiple [34] orientations have been considered. The backprojections of the acquired images on this surface are *locally* compared as to their visual similarity and the results are stored in a 2D similarity map. A depth-ordered stack of such similarity maps is generated and for each column along depth, the depth at which similarity is maximized is considered to signify the occurrence of the imaged surface. The backprojection and local comparison of images are operations that quite fit in the

single-instruction multiple-data architecture, of commodity graphics hardware. Thus a variety of GPU-accelerated space-sweeping techniques can be found in the literature, for example, [28, 29, 35].

Regarding the size of the backprojection surface in space-sweeping approaches, it has been shown [26] that projectively expanding this surface (as in [26–30]) exploits better the available pixel resolution, than implementing the sweep as a simple translation of the sweeping plane [25, 32, 35–39]. This projective expansion is adopted by the approach proposed in Section 3 and extended for the volumetric case in Section 4.

3. Maximizing the Number of Sampled Pixels for a Unit Backprojection Area

To indicate that the maximization of the number of sampled pixels per unit of backprojection area is directly related with the accuracy of reconstruction, the plane sweeping approach is reviewed. The main reason to select this approach is due to its practical applicability in obtaining successful stereo results in binocular or combination of binocular approaches (e.g., [28, 34, 40, 41]).

The observation that is brought forward is illustrated in (Figure 2, (left)). A planar backprojection surface is increasingly slanted to an intersecting line of sight as this line rotates from the center (coinciding then with the optical axis) to the periphery of the image. Thus, a unit area of this surface subtends more pixels when in the center of the image than in its periphery. (In monocular vision, rather than simulated backprojection, this effect is called “foreshortening” and refers to the transformation of the apparent size and shape of a surface when the viewpoint of observation is varied.) It is thus clear that the number of sampled pixels for a unit of backprojection-surface area is maximized, when this unit surface is frontoparallel to the line of sight from the camera to it.

The main difference of the proposed approach to planar space sweeping is that the backprojection surface is modified from planar to spherical. In addition, instead of performing the search for local similarity maxima in the “depth” direction, this search is performed along the direction of sight; that is, along expanding spherical sectors, as opposed to cubic voxels.

Using a spherical backprojection surface, a line of sight \vec{t} departing from the cyclopean optical center is always perpendicular to the backprojection surface for any eccentricity ϵ within the field of view (FOV) (see Figure 2). The number of sampled image pixels per unit area of backprojection surface is maximal and independent of eccentricity. In contrast, a planar frontoparallel backprojection surface is projected with increasing slant relatively to \vec{t} as ϵ moves to the periphery of the image. To illustrate the above, a small area on the backprojection surface is assumed as locally planar. As shown in Figure 2, the subtended visual angle of this area is maximized at the perpendicular posture CD . In any other posture (e.g., AB for plane sweeping), this angle is smaller since the image area subtended is decreased by a factor of $\cos(CpA)$ in *both* tilt and slant dimensions.

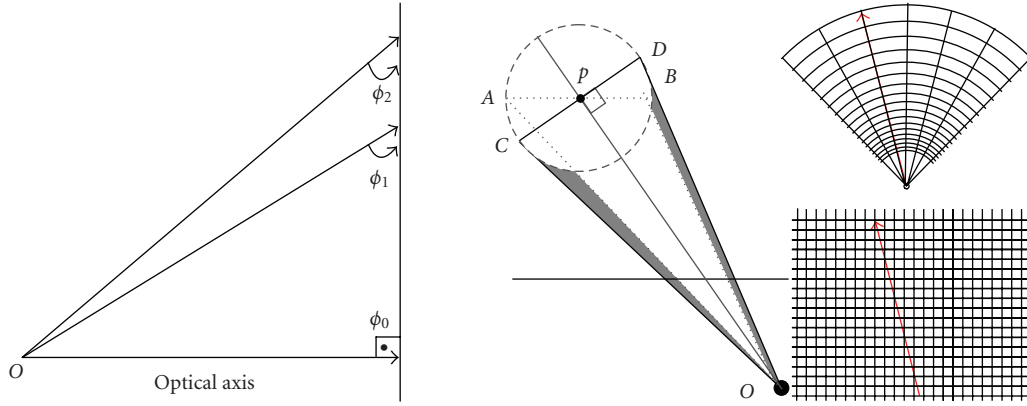


FIGURE 2: Flatland illustrations of the geometry of sphere sweeping. Left: A line of sight intersects a frontoparallel surface with increasing slant, as it moves from the center of the image (ϕ_0) to its periphery (ϕ_1, ϕ_2). Center: The subtended visual angle of a small area centered at p is maximized when this area is perpendicular to the line of sight from the projection center \vec{o} to \vec{p} and is less otherwise. Right: Illustrations of the sector- (top) and voxel- (bottom) based volume tessellations. Visibility is naturally expressed in the first representation, whereas in the second, traversing voxels obliquely is required for its computation.

3.1. Method Formulation. Let a series of concentric and expanding spheres emanating from the cyclopean eye \vec{o} , with corresponding radii d_i . Let also the cyclopean view frustum \mathcal{F} from the cyclopean eye. The intersection of \mathcal{F} with the spheres produces the spherical parallelograms, or sectors, S_i . The angular openings (μ, λ) of the spherical segments are matched to the horizontal and vertical FOVs of the cameras.

The concentric instances of the backprojection sector at depth values d_δ are noted as S_i . The set of d_i 's values is called depth range \mathcal{D} and $i \in \{1, 2, \dots, n\}$. Values d_i are exponentially increasing, so that the images' depth granularity is fully exploited, while a minimum number of depth values is evaluated [42]. Points on S_i are parameterized by an angular step of c and determined by spherical coordinates ψ and ω . Parameterization variables ψ and ω are determined as $\psi \in \{c \cdot i - \mu; i = 0, 1, 2, \dots, 2\mu/c\}$ and $\omega \in \{c \cdot j - \lambda; j = 0, 1, 2, \dots, 2\lambda/c\}$ and $[\mu/c] = \mu/c$, $[\lambda/c] = \lambda/c$. Angle ψ varies on the xz and ω on the yz plane. For both ψ and ω , value 0 corresponds to the orientation of the mean optical axis \vec{e} . To generate sectors S_i , a corresponding sector S_0 is first defined on a unit sphere. A point $\vec{p} = [x \ y \ z]^T$ on S_0 is given by $x = \sin(\psi)$, $y = \cos(\psi)\sin(\omega)$, $z = \cos(\psi)\cos(\omega)$. Its corresponding point \vec{p}_b on S_i is then

$$\vec{p}_b = d_i [R_z(-\psi)R_y(-\omega)\vec{p} + \vec{o}], \quad (4)$$

where R_y and R_z are rotation matrices for rotations about the yy' and zz' axes. The backprojection images are locally compared with a $w \times w$ correlation kernel \mathcal{K} , which yields a similarity score s . The strongest local maximum of s along a line of sight indicates the estimated depth. The requirement of locality for this maximum introduces robustness to spurious maxima and textureless regions.

The remainder of the sweeping procedure is conventional. For each S_i , the stereo images (≥ 2) are sampled at the projection S_i 's points on the acquired images, thus forming two ($2\mu/c \times 2\lambda/c$) backprojection images, which are locally compared. The similarity values are associated to the nodes

of a sector-interpretable grid (Figure 2, (right)), but whose data are structured in memory in a conventional 3D matrix.

Notice that both sphere and plane sweeping can be represented on a per voxel basis by the volumetric geometry formulated in Section 2. Sphere sweeping is represented by simply considering only the line of sight $\vec{t} = \vec{p} - \vec{o}$ as the value of \vec{n} in (2) and (3). To implement plane sweeping, \vec{n} is always parallel to the optical axis, rather than the line of sight. The shape of the surface is, then, implicitly defined by the direction of $\vec{\kappa}$ at which local maxima are detected within s .

Computational power is conserved in two ways. The first way is by precomputing the pencil of vectors from \vec{o} to the parameterized locations on S_0 at initialization and reusing this result at the computation of S_i at each depth. This pencil corresponds to $R_z(-\theta)R_y(-\phi)$ in (4), which is also the most computationally demanding component of this equation due to the matrix multiplication and trigonometric operations. The second way is by reducing the number of evaluated depth layers to the number of depths that can be sensed by the given stereo system. For a binocular pair, this means to parameterize d_i in steps which correspond to a binocular disparity of 1. In turn, this results in parameterizing d_i exponentially as $d_i = d_0 + \beta^i$, $i = 1, 2, \dots, i_N$, where d_0 and i_N define the sweeping interval and β is modulated so that the farthest distance is imaged in the available image resolution [42]. Memory is conserved similarly to [25], where a buffer that stores only the similarity result for each depth is utilized. A difference of the proposed approach is that it buffers the similarity result of both the previous and the next depths, in order to determine if the maximum is truly local. Finally, a second-order polynomial is fit around similarity maxima and in the direction of search, to accurately increase the precision of the reconstruction, in between depth intervals.

3.2. Experiments. The proposed approach was compared to plane sweeping on the same binocular pairs and experimental conditions. The scene imaged in each binocular pair

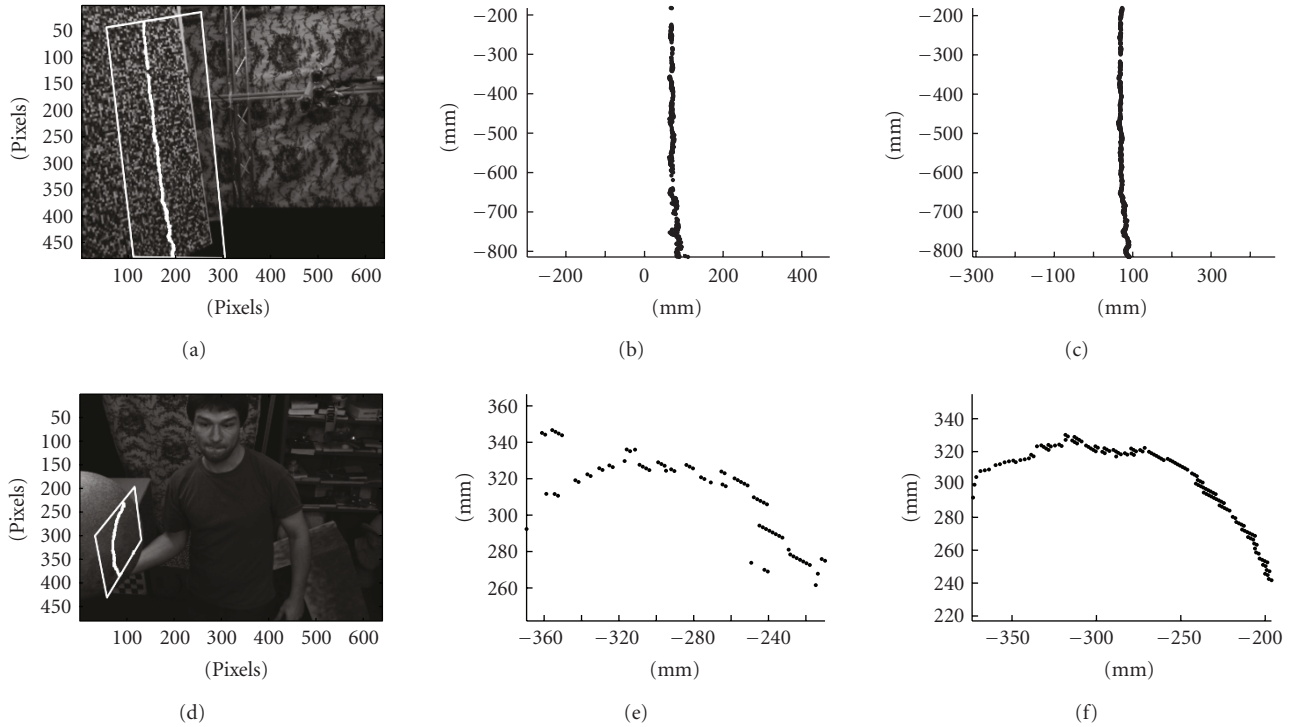


FIGURE 3: Comparison of planar and spherical backprojection surfaces in space sweeping. Each row shows an image from a binocular pair and sections of the obtained reconstructions for planar (center) and spherical (right) backprojection surfaces. In the experiment, $\tau = \cdot 7$, $FOV = \pi/4, \pi/4$, tessellation of d_i was 2 mm and regular. The stereoscopic image pair was obtained from a 156 mm-baseline camera pair. The images were fully calibrated images and rectified for lens distortion.

was reconstructed independently by plane-sweeping and the proposed sphere-sweeping methods.

To indicate differences among the results, a section extracted from each reconstruction at the same coordinates is presented. The sections were planar, vertical, and in the direction of sight. In Figure 3, two such comparisons are shown. In the top row, the section is close to the central image column of the images of the stereo pair. In the bottom row, the section corresponds to the periphery of the images. More comparative experiments can be found in [26].

A small improvement effect between the two methods can be observed in the reconstructions, when obtained from the center of images (top row). As expected, the improvement due to the spherical backprojection surface is most intensely pronounced when comparing reconstructions obtained from the periphery of images (bottom row). In terms of reconstructed area, sphere sweeping provided about $\approx 15\%$ more reconstructed points. A more quantitative confirmation of this result can be found in [26], where the evaluation of the reconstructions involved comparing the reconstruction result to an independently acquired 3rd image.

3.3. Discussion. Through the presented experiments, the expected accuracy improvement due to the utilization of a spherical backprojection surface versus planar space-sweeping has been demonstrated. In particular, this improvement is most intensely pronounced in the reconstruction of surfaces that occur in the periphery of the image, because in

this condition the backprojection plane is not perpendicular to the line of sight, and thus undersampled. It is stressed that, other than the change in the shape of the backprojection surface, no other algorithmic modifications to planar space-sweeping have been introduced in this technique. Therefore, the execution of the proposed technique can be accelerated in the GPU in the same way that planar space sweeping is [28, 29, 35]. Also for much wider-baseline arrangements, it has to be further studied whether the spherical surface should be elongated to form a conic with three fixed points that pass through the image centers [27], because then the line of sight is not to the backprojection surface, and thus the periphery is still undersampled.

For a binocular pair, parameterizing the reconstruction volume into sectors instead of voxels provides a practical surface parameterization for two reasons. First, because the data required to compute visibility are already structured with respect to visibility from the optical center. These data refer to a sector-interpretable grid (see Figure 2, (right)), but are structured in memory as a conventional 3D matrix. Application, then, of visibility rules becomes more accurate, because the oblique traversal of a regular voxel space, which leads to discretization artifacts, is avoided. Second, because the spatial granularity of surface discretization in the reconstruction is a function of image resolution, not world coordinates. Therefore, at greater distances, less representational capacity is required to represent the imaged surface, but still at the same detail.

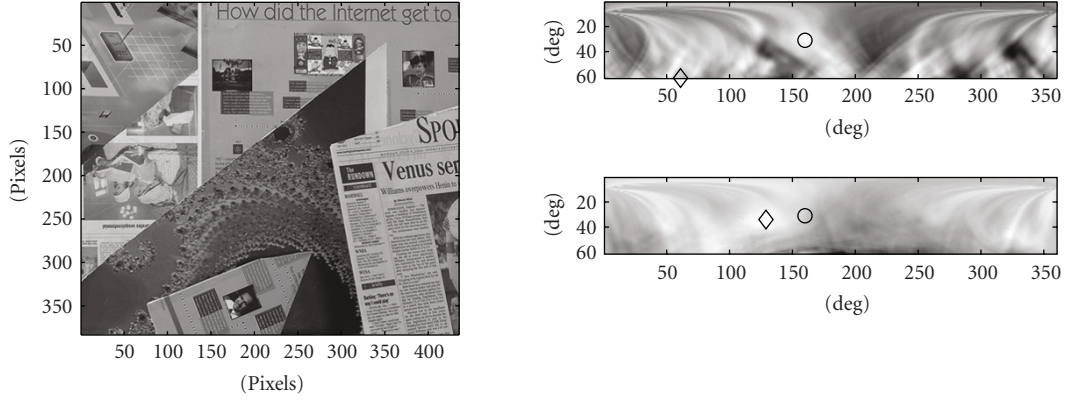


FIGURE 4: Accuracy evaluation of the patch operator using the first two frames of the “Venus” middlebury sequence. In the left figure, an image of the binocular pair is shown with the target point of the experiment marked by a dot. The right figures show the similarity maps obtained from the two experimental conditions: the top map shows the response of a constant-sized patch and the bottom map shows the response with size-modulation. In these maps, diamonds mark the estimated normal and circles the ground truth. In the experiment, $\alpha = 250$ length units, baseline was 100 length units, and $r = 151$. The projection of \mathcal{S} subtended ≈ 50 pixels in the image.

4. Size-Modulation of Volumetric Backprojection Surfaces

Volumetric approaches optimize the local orientation of the backprojection surface on a per voxel basis, as in (2) and (3). At a given point \vec{p} , the number of image pixels subtended \mathcal{S} is analogous to its obliqueness, or specifically, to the reciprocals of distance squared and the cosines of relative tilt and slant of \mathcal{S} to the cameras. When α is constant, the greater the obliqueness of \mathcal{S} , the fewer the image pixels that the $(r \times r)$ image samples for $w_{1,2}$ are obtained from. Therefore, there will always be a level of obliqueness above which the same image intensity values will be sampled multiple times. After this level, as obliqueness and/or distance continue to increase, the population of these intensities will tend to exhibit reduced variance. The reason is that the compared intensity values are being sampled from decreasingly fewer pixels, or otherwise, the same pixels are sampled multiple times. As a result, variance is artificially reduced. Thus when α is constant, a bias is predicted in the similarity function in favor of greater slants and distances. The mathematical reason of this bias is that variance occurs in the denominator of the correlation function. The intuitive explanation is that fewer image area supports now the similarity matching of backprojections on \mathcal{S} and, as a consequence, this matching becomes less robust to lack of resolution.

In this section, a modulation of α that casts the apparent (image) size of \mathcal{S} invariant to distance and obliqueness is proposed. Its effect is that pairs of compared collineations correspond to the same image area, which is shown to be important in the estimation of the imaged surface’s normal.

4.1. Method Formulation. The size α of \mathcal{S} is modulated so that the image area at which \mathcal{S} is projected remains invariant, while \mathcal{S} is hypothesized at different postures and distances from the cameras. In particular, the side of \mathcal{S} (or diameter,

for a circular \mathcal{S}) is modulated as

$$\alpha = \frac{\alpha_0 \cdot d}{d_0 \cdot \cos \omega}; \quad \omega = \cos^{-1} \left(\frac{\vec{v} \cdot \vec{n}}{|\vec{v}| \cdot |\vec{n}|} \right), \quad (5)$$

where $\vec{v} = \vec{p} - \vec{o}$, $d = |\vec{v}|$, ω is the angle between \vec{v} and \vec{n} and d_0 , α_0 initial parameters in units of world length. In the above equation, $(\cos \omega)^{-1}$ normalizes for changes in posture, d/d_0 for changes in distance and, as in Section 3, d_0 is a constant which determines the closest considered distance (or in an epipolar system, the largest considered disparity). Finally, notice that even for a single location α is still a variable of \vec{n} .

4.2. Experiments. The proposed approach was tested in both the angular and spatial domain, in two corresponding experiments. In the first, the increment in the accuracy of surface normal estimation at a single point is demonstrated. In the second, the responses of the operator with and without size modulation are compared, across the spatial extent of a scene. A more detailed description of these experiments can be found in [43].

In Figure 4, the improvement in estimating the surface normal of a surface, induced by the proposed size-modulation, is shown. In the figure, the responses obtained from the same patch operator with and without size-modulation are compared as to their accuracy. In the experiment, a point on an imaged surface was selected and the patch operator was centered and applied to this point. The corresponding similarity values $\text{sim}(w_1(\vec{p}, \vec{n}), w_2(\vec{p}, \vec{n}))$ are shown in a longitude-latitude parameterization of \vec{n} , with latitude corresponding to the horizontal axis. In the maps, camera pose \vec{c} is at $(0, 0)$, crosses mark the maximal similarity value, and circles mark ground truth. The expected improvement in accuracy induced by the proposed size-modulation is confirmed in the experiment, by the greater accuracy of the second condition. Notice that in the constant-size condition, the global maximum occurred at the border

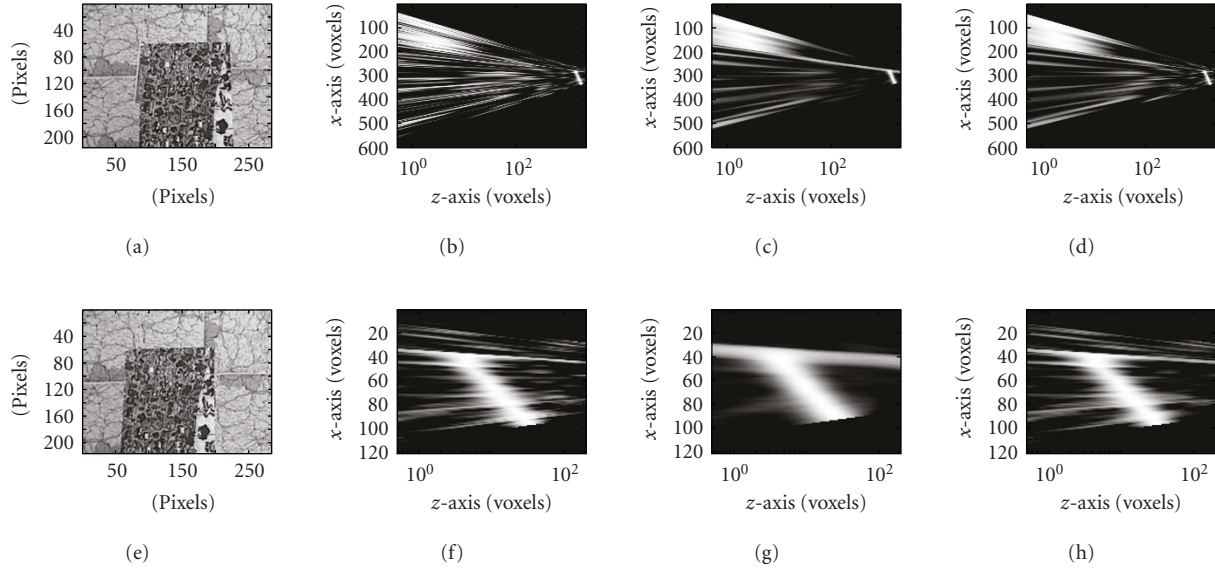


FIGURE 5: Shown is “Map” middlebury stereo pair (left column) and three separate calculations of s across a vertical section, through the middle of the foreground surface. The bottom figures are zoom-in details on the part that corresponds to the foreground surface in the image pair. The z -axes (horizontal in maps) are logarithmic. In the bottom figures, ground truth is marked with a dashed line. Columns 2 and 3 (from the left) correspond to the small and large α , respectively. The right column shows the response of for the size-modulated α .

of this map, at a posture more oblique than ground truth. This type of spuriously high-similarity values is expected, because at very oblique poses relative to the optical axis, the patch projects to just a few pixels.

The second experiment shows the increment in the accuracy of the volumetric similarity function s across the spatial extent of a scene. This similarity function, s , was evaluated for all the points of a reconstruction volume in three conditions; a small, a large, and a size-modulated α (see Figure 5). In the 2nd column, a fine α was used, hence the noisy response at the background. Using a larger α (3rd column) yields a smoother response in greater distances, but diminishes any detail that could be observed in short range. In the 4th column, α is projectively increased, thus normalizing the precision of reconstruction by the area that a pixel images at that distance. In the bottom figures, ground truth is marked with a dashed line.

The same effect is more intensely pronounced when the scene exhibits a greater range of depth. In the experiment of Figure 6, the performance of a constant α is compared against a size-modulated α for a scene that features ≈ 15 m of depth. In the experiment, the size modulation of α yields a less noisy correlation response, particularly at greater distances than a constant α .

4.3. Discussion. In this section, it is argued that modulating the size of a backprojection planar patch operator so that the patch projects at an equal amount of image area for each location and orientation produces more accurate results than when retained constant. The increase in robustness of the proposed approach versus approaches that utilize a patch of constant size was confirmed through reconstruction experiments, where ground truth was known.

Besides the importance of the accuracy of surface localization, the accuracy of surface normal estimation is important in reconstruction algorithms, because it facilitates accuracy in the final reconstruction as well [17]. Volumetric stereo algorithms utilize the readings of the planar patch operator \mathcal{S} in different ways. For example, in [18] similarity values are provided to a global optimization, the result of which is an isosurface that represents the reconstructed surface. In [22] besides texture similarity, photometrical properties are also computed on the patch and a multidimensional optimization is employed to determine the occupied voxels. In [23, 24], spatially local maxima in the response of the operator are regarded as a cue to surface occurrence. It is, thus, argued that the proposed modulation can be directly adopted by volumetric methods, such as the above, that utilize a constant-size hypothetical patch.

5. Conclusion

In this paper, the resolution effects of image backprojection for the implementation of the texture uniqueness cue have been studied, and methods to utilize image resolution more efficiently, in this process, have been proposed. The proposed techniques target the accuracy of results that are required in 3D TV applications, based on size and shape modulations of the backprojected surfaces. The volumetric representation of the output and the estimations of surface normals facilitate surface interpolation techniques that boost precision and rendering quality [23]. The common notation and locality of the proposed approaches have facilitated their sequential integration into a highly parallelizable computational module, which is utilized as a software engine for the production of 3D video for free-viewpoint rendering [17].

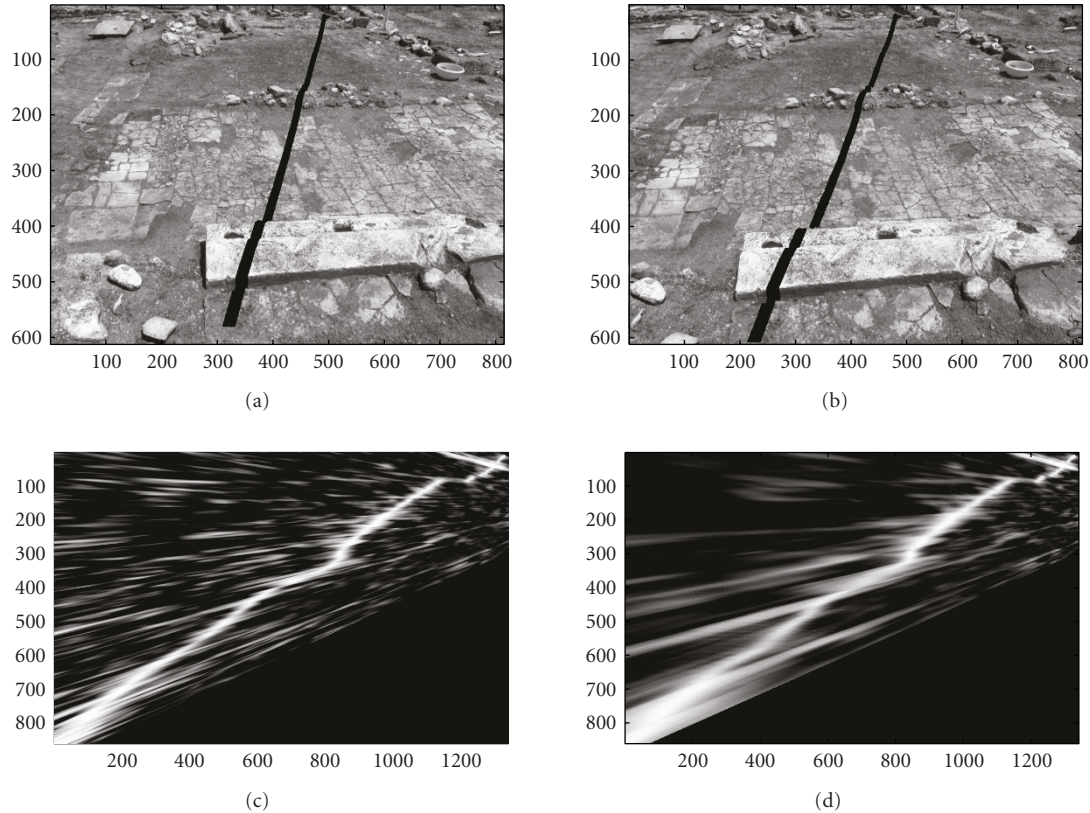


FIGURE 6: Shown on the top row is a stereo pair and on the bottom row two separate calculations of s across a vertical section, along the xx' axis of the scene. The section is indicated on the top row images by projecting the reconstructed points along this section back to the original images. In the bottom row, the left image corresponds to a constant α and the right to a size-modulated α .

The ability to commonly formulate the methods of Sections 3 and 4 facilitates the integration of the two proposed approaches in a coarse to fine estimation of regions of interest within \vec{V} . In this system [17], \vec{V} is initially approximated by a sweeping technique at coarse scale. The local maxima at that scale are utilized to determine volumetric (3D) regions of interest at which \vec{V} is to be recomputed at higher resolution and angular precision, using the optimization of (2) and (3). To seamlessly achieve this integration, the spherical sweeping approach is formulated on a per voxel basis as shown in Section 2. The per voxel estimations of \vec{V} from the sweeping process are then utilized as initial estimations that constrain the angular and spatial search spaces.

The volumetric locality of \vec{V} 's computation permits the volumetric partitioning of data for the parallelization of the process. In fact, the computation of \vec{V} is parallelizable not only on a per voxel, but also on a per evaluated orientation basis (i.e., for every \vec{n} in (2)). However, because surfaces occur only in the minority of voxels of a reconstruction volume, efficiently balancing the computational load across a number of computational resources is a topic of future study. The challenge is to dynamically focus on computational resources at the regions of interest, while also distributing appropriately the amounts of computation to minimize response time. In this domain, the most efficient distribu-

tion of computation among CPU and GPU computational resources is also a topic that remains to be studied.

The utilization of a volumetric representation, such as \vec{V} , and the estimation of surface normals are crucial to the fusion of multiple views [23]. When fusing input from multiple views, errors in camera registration due to calibration noise produce inaccuracies and duplicate occurrences of the same surface [15]. To cope with the task of merging multiple views, similarity scores are fused in a common voxel grid [23]. More recently, other such fusion approaches have been formulated, for example, [41, 44]. The present work is of service to the above approaches in enhancing the veridity of the readings of the fused volumetric similarity operators.

Another future direction of this work is in the integration of the computational findings regarding the accuracy of the volumetric patch operator with works that utilize such operators as discussed in Section 4.3. Most importantly, the ability of volumetric approaches to represent the intermediate results in a local basis facilitates the integration with other cues to shape those can be essential to the goals of scene reconstruction. For example, shape-from-silhouette is a method that can constrain significantly the search space while shape-from-shading and space carving can be the two of the few choices for surface reconstruction at textureless image areas. Moreover, constraints that arise from the detection of characteristic structures, such as planes [45,

46], and even from monocular perspective cues [47, 48] can significantly constrain the search space and prune outliers.

Acknowledgment

The authors are grateful for support through the 3D TV European NoE, 6th Framework IST Programme.

References

- [1] M. Levoy and P. Hanrahan, "Light field rendering," in *Proceedings of the 23rd Annual Conference on Computer Graphics and Interactive Techniques (SIGGRAPH '96)*, pp. 31–42, New Orleans, La, USA, August 1996.
- [2] D. Marr and T. Poggio, "Cooperative computation of stereo disparity," *Science*, vol. 194, no. 4262, pp. 283–287, 1976.
- [3] D. Marr and T. Poggio, "A computational theory of human stereo vision," *Proceedings of the Royal Society of London B*, vol. 204, no. 1156, pp. 301–328, 1979.
- [4] A. S. Ogale and Y. Aloimonos, "Stereo correspondence with slanted surfaces: critical implications of horizontal slant," in *Proceedings of the IEEE Conference on Computer Vision and Pattern Recognition (CVPR '04)*, vol. 1, pp. 568–573, Washington, DC, USA, June–July 2004.
- [5] M. Z. Brown, D. Burschka, and G. D. Hager, "Advances in computational stereo," *IEEE Transactions on Pattern Analysis and Machine Intelligence*, vol. 25, no. 8, pp. 993–1008, 2003.
- [6] D. Scharstein and R. Szeliski, "A taxonomy and evaluation of dense two-frame stereo correspondence algorithms," *International Journal of Computer Vision*, vol. 47, no. 1–3, pp. 7–42, 2002.
- [7] A. Laurentini, "The visual hull concept for silhouette-based image understanding," *IEEE Transactions on Pattern Analysis and Machine Intelligence*, vol. 16, no. 2, pp. 150–162, 1994.
- [8] G. K. M. Cheung, T. Kanade, J.-Y. Bouguet, and M. Holler, "A real time system for robust 3D voxel reconstruction of human motions," in *Proceedings of the IEEE Conference on Computer Vision and Pattern Recognition (CVPR '00)*, vol. 2, pp. 714–720, Hilton Head Island, SC, USA, June 2000.
- [9] V. Kolmogorov and R. Zabih, "Multi-camera scene reconstruction via graph cuts," in *Proceedings of the 7th European Conference on Computer Vision (ECCV '02)*, pp. 82–96, Copenhagen, Denmark, May 2002.
- [10] M. Okutomi and T. Kanade, "A multiple-baseline stereo," *IEEE Transactions on Pattern Analysis and Machine Intelligence*, vol. 15, no. 4, pp. 353–363, 1993.
- [11] K. N. Kutulakos and S. M. Seitz, "A theory of shape by space carving," *International Journal of Computer Vision*, vol. 38, no. 3, pp. 199–218, 2000.
- [12] W. Culbertson, T. Malzbender, and G. G. Slabaugh, "Generalized voxel coloring," in *Proceedings of the International Workshop on Vision Algorithms: Theory and Practice*, pp. 100–115, Corfu, Greece, September 1999.
- [13] G. G. Slabaugh, W. B. Culbertson, T. Malzbender, M. R. Stevens, and R. W. Schafer, "Methods for volumetric reconstruction of visual scenes," *International Journal of Computer Vision*, vol. 57, no. 3, pp. 179–199, 2004.
- [14] J. Lanier, "Virtually there," *Scientific American*, vol. 284, no. 4, pp. 66–75, 2001.
- [15] J. Mulligan, X. Zabulis, N. Kelshikar, and K. Daniilidis, "Stereo-based environment scanning for immersive telepresence," *IEEE Transactions on Circuits and Systems for Video Technology*, vol. 14, no. 3, pp. 304–320, 2004.
- [16] N. Kelshikar, X. Zabulis, J. Mulligan, et al., "Real-time terascale implementation of tele-immersion," in *Proceedings of the International Conference on Computational Science (ICCS '03)*, pp. 33–42, Melbourne, Australia, June 2003.
- [17] X. Zabulis and G. Kordelas, "Efficient, precise, and accurate utilization of the uniqueness constraint in multi-view stereo," in *Proceedings of the 3rd IEEE International Symposium on 3D Data Processing, Visualization and Transmission (3DPVT '06)*, pp. 137–144, Chapel Hill, NC, USA, June 2006.
- [18] O. Faugeras and R. Keriven, "Complete dense stereovision using level set methods," in *Proceedings of the 5th European Conference on Computer Vision (ECCV '98)*, vol. 1, pp. 379–393, Freiburg, Germany, June 1998.
- [19] S. Paris, F. X. Sillion, and L. Quan, "A surface reconstruction method using global graph cut optimization," *International Journal of Computer Vision*, vol. 66, no. 2, pp. 141–161, 2006.
- [20] J. Kim, V. Kolmogorov, and R. Zabih, "Visual correspondence using energy minimization and mutual information," in *Proceedings of the 9th IEEE International Conference on Computer Vision (ICCV '03)*, vol. 2, pp. 1033–1040, Nice, France, October 2003.
- [21] I. J. Cox, S. L. Hingorani, S. B. Rao, and B. M. Maggs, "A maximum likelihood stereo algorithm," *Computer Vision and Image Understanding*, vol. 63, no. 3, pp. 542–567, 1996.
- [22] R. L. Carceroni and K. N. Kutulakos, "Multi-view scene capture by surfel sampling: from video streams to non-rigid 3D motion, shape and reflectance," *International Journal of Computer Vision*, vol. 49, no. 2–3, pp. 175–214, 2002.
- [23] X. Zabulis and K. Daniilidis, "Multi-camera reconstruction based on surface normal estimation and best viewpoint selection," in *Proceedings of the 2nd International Symposium on 3D Data Processing, Visualization, and Transmission (3DPVT '04)*, pp. 733–740, Thessaloniki, Greece, September 2004.
- [24] A. Bowen, A. Mullins, R. Wilson, and N. Rajpoot, "Light field reconstruction using a planar patch model," in *Proceedings of the 14th Scandinavian Conference on Image Analysis (SCIA '05)*, pp. 85–94, Joensuu, Finland, June 2005.
- [25] R. T. Collins, "A space-sweep approach to true multi-image matching," in *Proceedings of the IEEE Conference on Computer Vision and Pattern Recognition (CVPR '96)*, pp. 358–363, San Francisco, Calif, USA, June 1996.
- [26] X. Zabulis, G. Kordelas, K. Mueller, and A. Smolic, "Increasing the accuracy of the space-sweeping approach to stereo reconstruction, using spherical backprojection surfaces," in *Proceedings of the International Conference on Image Processing (ICIP '06)*, pp. 2965–2968, Atlanta, Ga, USA, October 2006.
- [27] M. Pollefeys and S. Sinha, "Iso-disparity surfaces for general stereo configurations," in *Proceedings of the 8th European Conference on Computer Vision (ECCV '04)*, pp. 509–520, Prague, Czech Republic, May 2004.
- [28] R. Yang, G. Welch, and G. Bishop, "Real-time consensus-based scene reconstruction using commodity graphics hardware," in *Proceedings of the 10th Pacific Conference on Computer Graphics and Applications (PCCGA '02)*, pp. 225–234, Beijing, China, October 2002.
- [29] M. Li, M. Magnor, and H.-P. Seidel, "Hardware-accelerated rendering of photo hulls," *Computer Graphics Forum*, vol. 23, no. 3, pp. 635–642, 2004.
- [30] V. Nozick, S. Michelin, and D. Arqus, "Image-based rendering using plane-sweeping modelisation," in *Proceedings of the International Association for Pattern Recognition—Machine Vision Applications (IAPR '05)*, pp. 468–471, Tsukuba, Japan, May 2005.

- [31] H. Moravec, *Robot Rover Visual Navigation*, Computer Science: Artificial Intelligence, UMI Research Press, Ann Arbor, Mich, USA, 1981.
- [32] K. N. Kutulakos and S. M. Seitz, "A theory of shape by space carving," *International Journal of Computer Vision*, vol. 38, no. 3, pp. 199–218, 2000.
- [33] J. Mulligan, V. Isler, and K. Daniilidis, "Trinocular stereo: a real-time algorithm and its evaluation," *International Journal of Computer Vision*, vol. 47, no. 1–3, pp. 51–61, 2002.
- [34] D. Gallup, J.-M. Frahm, P. Mordohai, Y. Qingxiong, and M. Pollefeys, "Real-time plane-sweeping stereo with multiple sweeping directions," in *Proceedings of the IEEE Conference on Computer Vision and Pattern Recognition (CVPR '07)*, pp. 1–8, Minneapolis, Minn, USA, June 2007.
- [35] C. Zach, A. Klaus, B. Reitinger, and K. Karner, "Optimized stereo reconstruction using 3d graphics hardware," in *Proceedings of the Workshop of Vision, Modelling, and Visualization (VMV '03)*, pp. 119–126, Munich, Germany, November 2003.
- [36] J. Bauer, K. Karner, and K. Schindler, "Plane parameter estimation by edge set matching," in *Proceedings of the 26th Workshop of the Austrian Association for Pattern Recognition*, pp. 29–36, Graz, Austria, September 2002.
- [37] C. Zach, A. Klaus, J. Bauer, K. Karner, and M. Grabner, "Modeling and visualizing the cultural heritage data set of Graz," in *Proceedings of the Conference on Virtual Reality, Archeology, and Cultural Heritage*, pp. 219–226, Glyfada, Greece, November 2001.
- [38] C. Zhang and T. Chen, "A self-reconfigurable camera array," in *Proceedings of the International Conference on Computer Graphics and Interactive Techniques (SIGGRAPH '04)*, p. 151, Los Angeles, Calif, USA, August 2004.
- [39] T. Werner, F. Schaffalitzky, and A. Zisserman, "Automated architecture reconstruction from close-range photogrammetry," in *Proceedings of the CIPA International Symposium*, Potsdam, Germany, September 2001.
- [40] I. Geys, T. P. Koninckx, and L. Van Gool, "Fast interpolated cameras by combining a GPU based plane sweep with a Max-flow regularisation algorithm," in *Proceedings of the 2nd International Symposium on 3D Data Processing, Visualization, and Transmission (3DPVT '04)*, pp. 534–541, Thessaloniki, Greece, September 2004.
- [41] M. Goesele, B. Curless, and S. M. Seitz, "Multi-view stereo revisited," in *Proceedings of the IEEE Conference on Computer Vision and Pattern Recognition (CVPR '06)*, vol. 2, pp. 2402–2409, New York, NY, USA, June 2006.
- [42] J.-X. Chai, X. Tong, S.-C. Chan, and H.-Y. Shum, "Plenoptic sampling," in *Proceedings of the 27th Annual Conference on Computer Graphics and Interactive Techniques (SIGGRAPH '00)*, pp. 307–318, New Orleans, La, USA, July 2000.
- [43] X. Zabulis and G. D. Floros, "Modulating the size of back-projection surface patches, in volumetric stereo, for increasing reconstruction accuracy and robustness," in *Proceedings of the True Vision Capture, Transmission and Display of 3D Video Conference (3DTV '07)*, pp. 1–4, Kos Island, Greece, May 2007.
- [44] M. Habbecke and L. Kobbelt, "A surface-growing approach to multi-view stereo reconstruction," in *Proceedings of the IEEE Conference on Computer Vision and Pattern Recognition (CVPR '07)*, pp. 1–8, Minneapolis, Minn, USA, June 2007.
- [45] M. I. A. Lourakis, A. A. Argyros, and S. C. Orphanoudakis, "Detecting planes in an uncalibrated image pair," in *Proceedings of the British Machine Vision Conference (BMVC '02)*, vol. 2, pp. 587–596, Cardiff, UK, September 2002.
- [46] M. Pollefeys, F. Verbiest, and L. Van Gool, "Surviving dominant planes in uncalibrated structure and motion recovery," in *Proceedings of the 7th European Conference on Computer Vision (ECCV '02)*, pp. 837–851, Copenhagen, Denmark, May 2002.
- [47] A. Saxena, S. Chung, and A. Y. Ng, "Learning depth from single monocular images," in *Proceedings of the 20th Annual Conference on Neural Information Processing Systems (NIPS '06)*, vol. 18, Vancouver, Canada, December 2006.
- [48] L. Bergen and F. Meyer, "A novel approach to depth ordering in monocular image sequences," in *Proceedings of the IEEE Conference on Computer Vision and Pattern Recognition (CVPR '00)*, vol. 2, pp. 536–541, Hilton Head Island, SC, USA, June 2000.